Article:
Haque, N and Mullis, AM orcid.org/0000-0002-5215-9959 (2019) Existence of seaweed structures in rapidly solidified Ni3Ge intermetallic. Journal of Alloys and Compounds, 801. pp. 640-644. ISSN 0925-8388

https://doi.org/10.1016/j.jallcom.2019.06.050

Existence of recrystallized and seaweed structures in rapidly solidified Ni_3Ge intermetallic

Nafisul Haque[1, 2], Andrew M. Mullis[1]

[1] School of Chemical & Process Engineering, University of Leeds, Leeds LS2 9JT, UK

[2] Department of Metallurgical Engineering, NEDUET, University Road, Karachi 75270, Pakistan

[a] Corresponding author: engrnafis@gmail.com, A.M.Mullis@leeds.ac.uk

Keywords: rapid solidification; intermetallic compound; dendritic microstructure, dendritic seaweed

The congruently melting, single phase intermetallic β-Ni_3Ge has been subject to rapid solidification via drop-tube processing. A range of morphologies are observed in this material including spherulites, dendrites (which may display either orthogonal or non-orthogonal side-branching), a recrystallized structure and dendritic seaweed with increasing departure from equilibrium. In the case of the seaweed structure only, a progressive transition from high undercooling morphologies near the nucleation point to low undercooling morphologies is evident as growth proceeds. This appears to indicate that unlike normal dendritic growth, seaweed growth does not reach a steady-state and may in fact be more akin to growth at a planar interface.

1. Introduction

In science, dendritic solidification has been a topic of lasting inquiry. This is due to dendrites being a primary example of spontaneous pattern formation. This is also because of the extensive influence of dendrites on the engineering properties of metals [1]. In metallurgy, a dendrite is a distinctive tree-like crystal structure formed when the molten metal freezes along favourable growth directions. As dendrites generally survive metallurgical processing operations, such as rolling and forging, the original dendritic structure formed during solidification can have a significant effect on the mechanical properties of finished metallic components [2].

The strong directionality that gives rise to dendrites during solidification has it's origins in the underlying crystalline anisotropy, which is manifest as a set of 'easy' growth directions. These are directions of minimum capillary stiffness (a quantity that represents the reduction of the melting temperature at the solid/liquid interface [3]) whereby the melting temperature is most highly depressed by the Gibbs-Thomson effect. Typically, for metals with an

underlying cubic symmetry, this gives rise to growth along the <100> directions resulting in six primary arms displaying well developed, orthogonal, side-branches.

A number of changes to this solidification structure may become apparent with increasing departure from equilibrium. That can be either a switch in the favoured growth direction or a more general loss of directionality in the solidification morphology resulting in the growth of dendritic seaweed or dense branched fractal structures [4]. Typically, the first of these leads to a switch from the equilibrium <100> growth direction, to growth along either the <110> or <111> directions. The <100> to <110> transition has been observed directly in the transparent analogue casting system NH_4Cl – H_2O [5]. In this transition the primary solidification morphology remains dendritic. However, the transition is evident by a switch to side-branches which are no longer orthogonal to the primary trunk. A number of metallic systems, including alloys of cubic metals such as Cu-Ni, have been observed to undergo a <100> to <111> growth transition with increasing departure from equilibrium [4, 6]. In metallographic section the dendrites now no longer appear to have the usual cubic symmetry as each equiaxed dendrite will now have 8 primary arms pointing towards the corners of the unit cube, rather than the more familiar 6 directed towards the cube faces. In some systems such a switch in the growth direction has also been observed to occur coincidently with a break in the gradient of velocity-undercooling curve [7].

β-Ni_3Ge is a congruently melting intermetallic compound with the $L1_2$ ordered fcc crystal structure and a homogeneity range of 22.5 to 25 at. % Ge. When subject to rapid solidification via drop-tube processing, a range of solidification morphologies are observed with increasing departure from equilibrium. These are, in order of increasing departure from equilibrium: spherulites (droplet diameter 850 – 500 μm, cooling rate 700 – 1400 K s^{-1}), mixed spherulites and dendrites (500 – 150 μm, 1400 – 7800 K s^{-1}), well-defined dendrites with orthogonal side-branching (150 – 106 μm, 7800 – 13000 K s^{-1}), dendrites with non-orthogonal side-branching (106 – 75 μm, 13000 – 24000 K s^{-1}), a crack-like microstructure, subsequently identified as having undergone recrystallisation (75 – 53 μm, 24000 – 42000 K s^{-1}) and dendritic seaweed (53 – 38 μm, 42000 – 62000 K s^{-1}) [8-11]. All of these morphologies can be seen from the **Figure 1**.

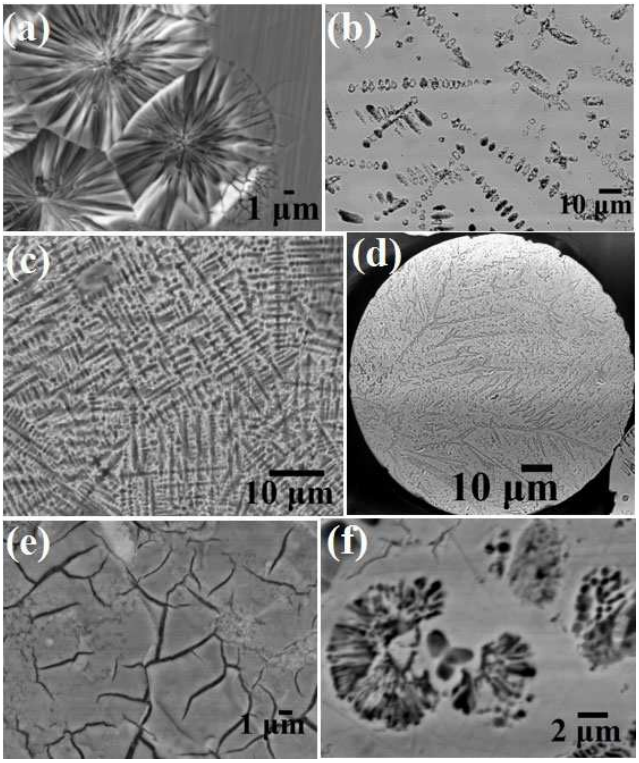

Figure 1: SEM micrograph of HF etched Ni_3Ge drop-tube samples (a) Spherulites, (b) mixed spherulites & dendrites (c) dendrites – orthogonal (d) dendrites - non-orthogonal, (e) crack-like (recrystallized), and (f) dendritic seaweed, are observed imbedded within a featureless matrix.

The contrast in these samples is visible only after etching in an aggressive mixture of HF, HCl and HNO_3. This differential etching does not appear to be due to change in phase, XRD analysis shows the material remains fully single phase β-Ni_3Ge irrespective of cooling rate. Nor is it due to any compositional difference, with EDX confirming that the material is chemically homogeneous and at the notional β-Ni_3Ge stoichiometry. In fact, Selected Area Diffraction Patterns (SADP) obtained in the TEM indicate that the only difference between the observed features and the surrounding matrix material is the degree of chemical ordering. Consequently, we observe a contrast between disordered material, which has preferentially dissolved in the etchant, relative to the ordered material which is relatively unetched. It appears that the observed features (spherulites, dendrites, seaweed) are the primary solidification morphology formed during the recalescence stage of solidification and have been subject to disorder trapping during rapid growth. These are therefore chemically disordered with the A1-fcc crystal structure. Subsequently, the rest of the material solidifies more slowly during the plateau phase of solidification, wherein growth of the chemically

ordered $L1_2$ phase occurs [12]. The underlying crystallography, as revealed by selected area diffraction analysis in the TEM, remains the same irrespective of cooling rate [10].

Spontaneous grain refinement (SGR) is also observed in the same congruently melting intermetallic compound β-Ni_3Ge. Microstructural and EBSD data provide compelling evidence of spontaneous grain refinement by recrystallization and recovery within a narrow size range of drop-tube processed, single phase β-Ni_3Ge powders spanning the range of cooling rates 24000 – 42000 K s^{-1}, 75 – 53 μm [11]. This recrystallization grain refinement is observed at lower undercooling than the transformation to dendritic seaweed structure. However, for very high cooling rates (> 42000 K s^{-1}) recrystallization is suppressed and frozen in seaweed structures are observed [10].

In this article we present an analysis of rapidly solidified Ni-23.8 at % Ge produced using the drop-tube technique, focusing on droplets in the 53 – 38 μm size range (cooling rate, 42000 – 62000 K s^{-1}) in which we observe a progressive change in the microstructure across the droplet, as solidification proceeds.

2. Experimental Methods

Congruently melting, single phase β-Ni_3Ge [13] was produced by arc melt Ni and Ge together under a protective argon atmosphere. To ensure homogeneity of the final compound, the arc-melting process was repeating 8 times with the phase composition of subsequent ingot being confirmed by X-ray diffraction using a PANalytical Xpert Pro. The data were collected over a range of 20-100° in 2θ, using Cu-K_α radiation (λ = 0.15418 nm) generated at an anode voltage of 40 kV and with a current of 40 mA.

Once the material was confirmed to be single phase, rapid solidification processing was undertaken using the Leeds 6.5 m drop-tube [8]. The arc-melt ingot, which was approximately 9.6 g in mass, was loaded into an alumina crucible which had three, 300 μm, laser drilled holes in the base. The sample was melted by using induction heating, with a graphite suseceptor being utilized in order to achieve efficient RF coupling. Once the desired temperature of 1480 K (1207 °C) (corresponding to 75 K superheat) was achieved the crucible was pressurized to 400 kPa wherein a spray of fine droplets is produced. These solidify in free fall down the tube, which is maintained at a pressure of 50 kPa with a high purity inert atmosphere. Further details of this drop-tube method are given in [8].

The Ni_3Ge drop-tube powders were prepared for analysis by mounting, grinding polishing and etching. First, the sieving into particle size ranges of the powders was performed. This was done by utilizing nine wire mesh stacking sieves that have apertures that decrease: ≥ 850 μm (< 700 K s^{-1}), 850 – 500 μm (700 –1400 K s^{-1}), 500 – 300 μm (1400 – 2800 K s^{-1}), 300 – 212 μm (2800 –4600 K s^{-1}), 212 – 150 μm (4600 – 7800 K s^{-1}), 150 – 106 μm (7800 – 13000 K s^{-1}), 106 – 75 μm (13000 – 26000 K s^{-1}), 75 – 53 μm (26000 – 42000 K s^{-1}), 53 – 38 μm (42000 – 62000 K s^{-1}) and ≤ 38 μm (> 62000 K s^{-1}). During sieving the sieve stack was agitated for 10 minutes. For each size fraction the cooling rate, calculated using the methodology described in [11], is shown in brackets. The mounting of the powder in a Trans Optic™ resin followed from its removal from all the sieves of varying size (≥ 850 μm to ≤ 38 μm).

XRD analysis was used to confirm that the drop-tube powders remained single-phase following rapid solidification processing. Subsequent to XRD analysis they were mounted and polished to a 0.5 μm surface finish for microstructural analysis. Following polishing the samples were etched using a mixture of equal parts of HF, HCl and HNO_3. A Carl Zeiss EVO MA15 scanning electron microscope (SEM) operating in secondary electron imaging mode was used to image the microstructure of the droplets revealed by etching while an Oxford Instrument X-Max Energy-Dispersive X-Ray (EDX) detector was used to check the chemical homogeneity of the samples. The EDX line scan technique was also used with same equipment on etched sample for the analysis of contrast between the microstructures and the featureless matrix. Electron backscatter diffraction (EBSD) was performed using a FEI Quanta 650 FEGSEM with EBSD and KE Centaurus system (Hillsboro, OR, USA).

3. Results and Discussion

The starting material for the drop-tube experiments was single phase β-Ni_3Ge, this being confirmed by XRD analysis on the polished surface of the arc-melted ingot. It can be seen from **Figure 2a** that all the XRD peaks may be reliably indexed to the β-Ni_3Ge phase using the ICCD reference pattern 04-004-3112. When similar material was deeply undercooled by Ahmad *et al.*, [14] using a melt fluxing technique, the resultant material also remained single phase for all undercoolings studied. XRD analysis reveals that the same is true during rapid cooling via drop-tube processing, with the drop-tube powders 850 μm – 150 μm [8], 75 – 53 μm [11] and 53 to ≤ 38 μm **(Figure 2a)** displaying peaks that can unambiguously be associated with the β-Ni_3Ge reference pattern.

EDX line scans, performed on HF etched samples, were used to confirm that the contrast observed upon etching was not being produced by compositional difference produced by partitioning during solidification. **Figures 2b** is an example of one such line scan, wherein it is clear that, to within the experimental position error associated with the technique, there is no variation in composition between the structures revealed by etching and the surrounding featureless matrix.

An SEM micrograph obtained from the polished and etched powder in the 53 – 38 μm sieve fraction is shown in **Figure 3a**. Four different morphologies may be observed within a same droplet, these being dendritic seaweed, crack-like (recrystallized), dendritic and featureless matrix. Each of these microstructures has been reported as occurring separately in this material previously, with each structure being associated with a different powder size range. However, what is unusual here is that structures spanning such a wide range of cooling rates, from seaweed that only occurs for $\dot{R} > 42000$ K s^{-1} to normal (orthogonal dendrites) which have previously been associated with cooling rate below 13000 K s^{-1}, should all occur in the same sample. In particular, the high undercooling morphology (dendritic seaweed) is located towards the bottom of the microstructure and appears to be radiating outwards from the lower right-hand corner of the image towards the upper left. As solidification proceeds the morphology appears to progress through various lower undercooling forms including recrystallized and dendritic, finally terminating with a significant fraction of featureless matrix. **Figure 3b** shows a second sample, also from the 53 - 38 μm size range. In this sample a similar transition from seaweed to dendritic growth can also be observed, although now with no evidence of the crack-like recrystallized morphology. Growth appears to have been nucleated on the left hand margin of the droplet and progressed towards the right-hand margin, with again a significant fraction of featureless matrix material towards the region where solidification would have terminated.

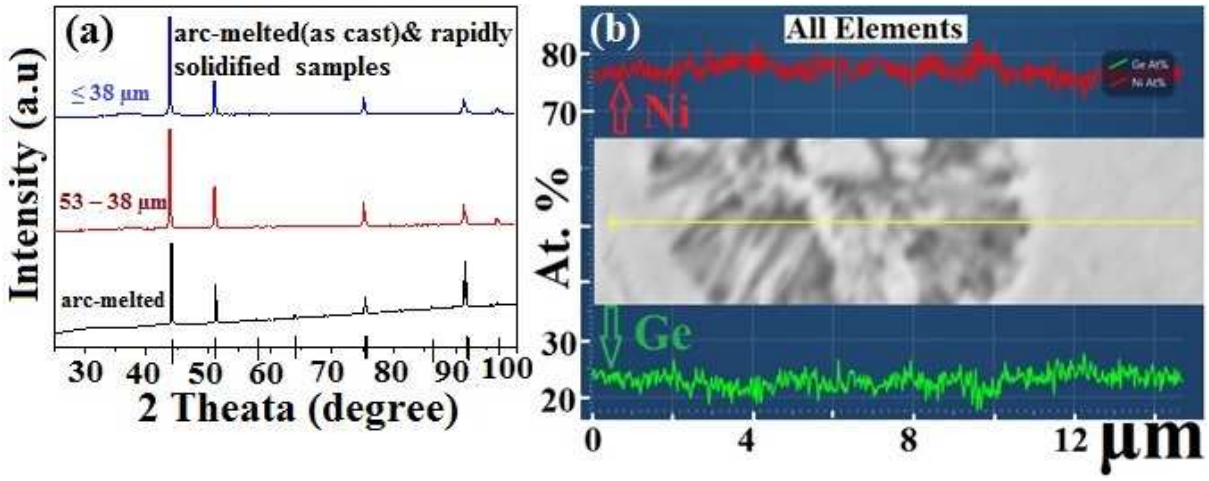

Figure 2: (a) X-ray diffraction analysis of an arc melted sample prior to drop-tube process (black) and two drop-tube processed powders of varying sizes. Vertical black lines indicate peak positions for the β-Ni_3Ge reference pattern and (b) EDX line scan across a dendritic seaweed trunk showing that the contrast revealed by etching is not the result of solute partitioning.

EBSD Euler mapping was also used to study the drop-tube samples in the size range 53 – 38 µm, as shown in the **Figure 4a**. Unfortunately, for EBSD analysis we require unetched samples and consequently it is not possible to guarantee that the image shown in **Figure 4a** corresponds to either of the shown in **Figure 3**. However, it does show some similar features. In particular, very fine grained material is apparent on one margin (around the 4-5 o' clock position), becoming more coarse grained towards the opposite side of the droplet. We have previously shown that seaweed microstructures tend to display large numbers of fine grains in EBSD, due to the growth not effectively following well defined crystallographic directions. Consequently, the EBSD map shown in **Figure 4a** is suggestive that a similar process is occurring in the droplet. The histogram grain orientations is shown in **Figure 4b** [15].

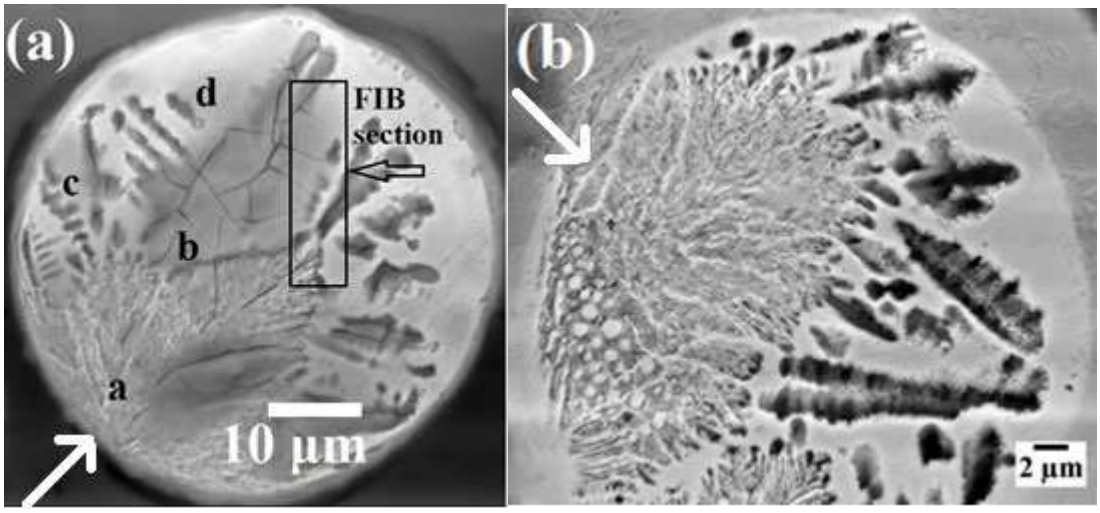

Figure 3: (a) SEM micrographs of HF etched β-Ni_3Ge drop-tube particles from the 53 – 38 µm size fraction showing dendritic seaweed, crack-like structure, dendrites and featureless matrix at a-d regions and (b) dendritic seaweed structure along with featureless matrix, within the same size of drop-tube particle (a).

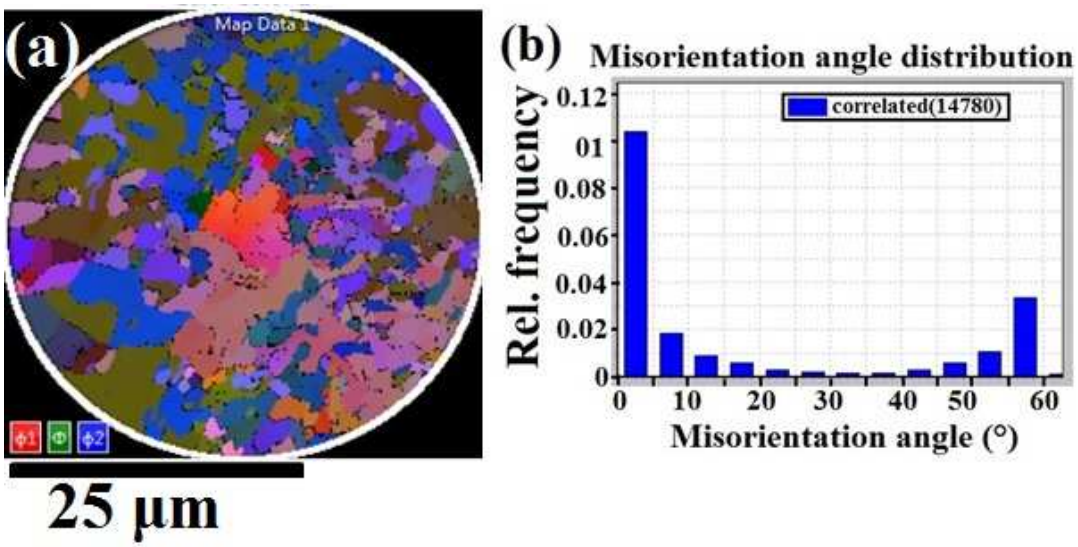

Figure 4: (a) Electron backscatter diffraction (EBSD) result of Euler texture map of unetched β-Ni_3Ge drop-tube particle size 53 – 38 µm and **(b)** Histogram of the correlated misorientation angle distribution across grain boundaries for the image shown in **(a)**.

During recalescence the material that has completed solidification will be at the melting temperature, T_m, and the material well ahead of this will be at a lower temperature, $T_m - \Delta T$. These two are separated by a thermal boundary layer. The width of which is typically $2\alpha/V$, where α is the thermal diffusivity (around 10^{-5} m^2 s^{-1}) and V is the growth velocity. In deeply

undercooled metals the growth velocity is high so the boundary layer will be small, typically << 1 μm and consequently there is no bulk warming of the sample as recalescence proceeds. However, we aware from the previous work of same compound that Ni_3Ge has low growth velocity. The velocity at the order-disorder transition undercooling of 168 K is just 0.22 m s^{-1}, rising to around 3.5 m s^{-1} at 350 K, which was the highest undercooling achieved [16]. Assuming here that we are well above the order-disorder transition undercooling and perhaps close to the 350 K achieved by Ahmed *et al*., we would estimate the thermal boundary layer as being of the order of 3 μm. This is insufficient to produce the effect observed here, whereby seaweed growth appears to be terminated around half way across the 53 - 38 μm droplets.

In rapid solidification experiments (levitation or drop-tube type experiments) which typically utilise relatively small droplets, each droplet will have a well-defined nucleation undercooling, wherein it will generally only display one type of solidification morphology. It is unusual to observe a range of solidification morphologies within a single sample. This is particularly the case for dendritic type structures which grow in a non-space filling manner. However, for these droplets in the 53 – 38 μm size range only, we observe a progressive change in the microstructure across the droplet, with the seaweed structure indicative of very high undercooling giving way to other lower undercooling morphologies as growth proceeds. Such transitions are generally only observed for structures which grow with a planar, space filling, interface such as eutectics. In these cases a transition from high to low undercooling morphologies as the growth proceeds is common, (see e.g. [17]) and is indicative of a solidification process for which a steady-state does not exist. The results presented here suggest a similar situation may occur during seaweed growth. This may indicate at high undercooling the dendritic seaweed morphology is growing in a manner more akin to that of space filling morphologies. This has significant implications for our understanding of seaweed, and other densely branched fractal, growth morphologies.

4. Summary & conclusion

Drop-tube processing has been used to rapidly solidify the congruently melting, single phase intermetallic compound β-Ni_3Ge within sample size range 53 – 38 μm. The corresponding range of cooling rates is 42000 – 62000 K s^{-1}. In this size fraction only we observe a progressive transition in growth morphology from a densely branched seaweed structure close to the apparent nucleation point to lower undercooling morphologies. This tendency

appears to be restricted to samples containing seaweed morphologies. We conclude that dendritic seaweed, and other densely branched fractal growth morphologies, may grow with a planar interface in a manner more akin to that of space filling morphologies such as eutectics.

Acknowledgments

Nafisul Haque is thankful to the Higher Education Commission (HEC) Pakistan and NED University of Engineering & Technology for financial support.

References

[1] A.M. Mullis, The origins of spontaneous grain refinement in deeply undercooled metallic melts, Metals, 4 (2014) 155-167.
[2] J.A. Dantzig, M. Rappaz, Solidification, EPFL press, 2009.
[3] H. Assadi, M. Oghabi, D. Herlach, Influence of ordering kinetics on dendritic growth morphology, Acta Materialia, 57 (2009) 1639-1647.
[4] E.G. Castle, A.M. Mullis, R.F. Cochrane, Evidence for an extensive, undercooling-mediated transition in growth orientation, and novel dendritic seaweed microstructures in Cu–8.9 wt.% Ni, Acta Materialia, 66 (2014) 378-387.
[5] Y. Sawada, Transition of growth form from dendrite to aggregate, Physica A, 140 (1986) 134-141.
[6] E.G. Castle, A.M. Mullis, R.F. Cochrane, Mechanism selection for spontaneous grain refinement in undercooled metallic melts, Acta Materialia, 77 (2014) 76-84.
[7] K. Dragnevski, R. Cochrane, A. Mullis, The solidification of undercooled melts via twinned dendritic growth, Metallurgical and Materials Transactions A, 35 (2004) 3211-3220.
[8] N. Haque, R.F. Cochrane, A.M. Mullis, Rapid solidification morphologies in Ni 3 Ge: spherulites, dendrites and dense-branched fractal structures, Intermetallics, 76 (2016) 70-77.
[9] N. Haque, R.F. Cochrane, A.M. Mullis, Morphology of Order-Disorder Structures in Rapidly Solidified L12 Intermetallics, in: TMS 2017 146th Annual Meeting & Exhibition Supplemental Proceedings, Springer, 2017, pp. 729-736.
[10] N. Haque, R.F. Cochrane, A.M. Mullis, Disorder-order morphologies in drop-tube processed Ni 3 Ge: Dendritic and seaweed growth, Journal of Alloys and Compounds, (2016).
[11] N. Haque, R.F. Cochrane, A.M. Mullis, The Role of Recrystallization in Spontaneous Grain Refinement of Rapidly Solidified Ni3Ge, Metallurgical and Materials Transactions A, 48 (2017) 5424-5431.
[12] N. Haque, R.F. Cochrane, A.M. Mullis, Morphology of Spherulites in Rapidly Solidified Ni3Ge Droplets, Crystals, 7 (2017) 100.
[13] A. Nash, P. Nash, Binary Alloy Phase Diagrams, in: US National Bureau of Standards Monograph Series 25, Elsevier, ASM, Ohio, 1976, pp. 35.
[14] R. Ahmad, R. Cochrane, A. Mullis, Disorder trapping during the solidification of β-Ni_3Ge from its deeply undercooled melt, Journal of Materials Science, 47 (2012) 2411-2420.
[15] J. Mackenzie, The distribution of rotation axes in a random aggregate of cubic crystals, Acta Metallurgica, 12 (1964) 223-225.
[16] R. Ahmad, R. Cochrane, A. Mullis, Disorder trapping during the solidification of βNi3Ge from its deeply undercooled melt, Journal of Materials Science, 47 (2012) 2411-2420.

[17] C. Clopet, R. Cochrane, A. Mullis, The origin of anomalous eutectic structures in undercooled Ag–Cu alloy, Acta Materialia, 61 (2013) 6894-6902.